Trends in High-Temperature H_2 Production on CeO_2 Co-Doped with Trivalent Cations in Solid Oxide Electrolysis Cells

Wu, Tiantian; Vegge, Tejs; Anton Hansen, Heine

Published in:
Journal of Catalysis

Link to article, DOI:
10.1016/j.jcat.2023.02.010

Publication date:
2023

Document Version
Publisher's PDF, also known as Version of record

Journal of Catalysis 420 (2023) 1–8

Contents lists available at ScienceDirect

Journal of Catalysis

journal homepage: www.elsevier.com/locate/jcat

Trends in high-temperature H_2 production on CeO_2 Co-doped with trivalent cations in solid oxide electrolysis cells

Tiantian Wu [a,b], Tejs Vegge [b,*], Heine Anton Hansen [b,*]

[a] School of Chemistry, Engineering Research Center of Energy Storage Materials and Devices of Ministry of Education, National Innovation Platform (Center) for Industry-Education Integration of Energy Storage Technology, Xi'an Jiaotong University, Xi'an 710049, China
[b] Department of Energy Conversion and Storage, Technical University of Denmark, Anker Engelunds Vej Building 301, 2800 Kgs. Lyngby, Denmark

ARTICLE INFO

Article history:
Received 29 November 2022
Revised 27 January 2023
Accepted 17 February 2023
Available online 18 February 2023

Keywords:
Correlations
Hydridic H-species
Oxygen diffusion barriers
Effect of potential
Relative position of dopants

ABSTRACT

CeO_2-based catalysts incorporated with cooperative dopants show excellent potential for promoting H_2 production via the water-splitting reaction (WSR) in solid oxide electrolysis cells (SOECs). Here, we report that CeO_2 co-doped with Gd + Sb, Pr + Sb, and Bi + Sb trivalent cations have superior performance for WSR with the reaction rate 2–5 orders of magnitude larger than that of individual trivalent dopants including Ga, Sb, Lu, Gd, Sm, Pr, Bi, and La, owing to improved stability of hydridic H-species and accordingly decreased barrier for their decompositions into H_2 by co-doping. The energy of hydridic H-species and the turn-over frequency (TOF) toward H_2 production is shown to correlate well with the average ionic radius of trivalent cations, where the TOF increases with decreasing ionic radius and Gd + Sb, Pr + Sb, and Bi + Sb with smaller ionic radius show better WSR activity than other dopants. Our studies suggest incorporating ceria with proper co-dopants with an average radius close to Gd + Sb, Pr + Sb, or Bi + Sb pairs as an effective strategy for enhancing WSR performance on CeO_2 in SOECs.

1. Introduction

The storage of renewable energy in the form of H_2 fuel via the WSR in SOECs is a sustainable way for energy storage and conversion [1–5]. The deployment of SOECs has been limited because of mechanical instability of cathodes and correspondingly decreased reactivity, owing to degradation at narrow gas/electrode/electrolyte reaction boundaries at a high operating temperature around 1200 K [1,2,4]. It is critical to developing both mechanically stable and kinetically active catalysts in cathodes of SOECs. Ceria-based materials have excellent ionic and electronic conductivity because ceria exposes a large ceria-gas reaction interface and is accessible for gas, electrons, and ions, which allows the stable operation at intermediate temperature (below 1200 K) and thus has been applied as cathodes for the WSR in SOECs [1–3,6,7].

For WSR in an SOEC, oxygen ions diffuse from the cathode to the anode to form oxygen gas, corresponding to the diffusion of oxygen vacancies from the deep layer to the top surface of the cathode [2,3]. Therefore, WSR on CeO_2 creates one oxygen vacancy in the subsurface, followed by the oxygen vacancy diffusion to the surface. Then, water adsorbs near the oxygen vacancy and dissociates into hydroxyls or hydridic H-species at the cathode [6,8]. Investigations on water dissociation over ceria for H_2 production have demonstrated that the fundamental reaction step of WSR on CeO_2 is the formation of hydroxyls or hydridic H-species (if hydrogen coverage is beyond one monolayer), followed by hydroxyl decomposition into H_2 [3,6,8–12]. There have been direct experimental observations of the formation of hydroxyls (O–H) or hydridic H-species (Ce-H) on CeO_2 during the reactions associated with water and hydrogen [13–15]. Our previous studies have identified an efficient reaction pathway for the WSR via the formation of hydridic H-species (Ce-H or dopant-H) on CeO_2 [6,8,10,12], where the total free energy barrier for H_2 production at 800 K via the formation of Ce-H on clean CeO_2 (1 1 1) surface is 2.91 eV. At the same time, it decreases to 2.66 eV by Gd doping because of the more favorable formation of Gd-H than Ce-H. Therefore, a key for further improving WSR on CeO_2 is to stabilize the formation of hydridic H-species, especially to promote the formation of dopant-H on CeO_2 by incorporating CeO_2 with proper dopants.

To facilitate the formation of hydridic H-species and improve the reaction kinetics of WSR on CeO_2 at intermediate temperature, incorporating dopants in CeO_2 holds excellent potential due to their positive effect on electronic structure, oxygen vacancy formation, ionic conductivity, and intermediate-temperature stability of ceria that have widely reported in SOECs [16–21]. Till now, many detailed investigations have been conducted on how individual dopants such as Gd, Sm, La, and Pr engineer the reactivity of ceria

* Corresponding authors.
E-mail addresses: teve@dtu.dk (T. Vegge), heih@dtu.dk (H. Anton Hansen).

https://doi.org/10.1016/j.jcat.2023.02.010
0021-9517/

[6,22–27]. In contrast, a few studies have explored co-doping strategies for promoting the H_2 production via WSR on ceria, and how co-dopants affect the formation of hydridic H-species (Ce-H or dopant-H) remains unclear. Our previous computational studies on the Pr and Bi (Pr + Bi) cooperative pair have given inspiration for using co-doping as an effective strategy for improving the WSR over CeO_2 because Bi and Pr co-dopants can effectively stabilize hydridic H-species and lower the barrier to produce H_2, leading to the significantly enhanced WSR activity compared to individual Pr, Bi or Gd dopant [28]. It has been reported that Pr + Bi co-doped ceria has lower activation energy than Gd-doped samples under wet 4% H_2 atmosphere, although good WSR performance was not always found because of the complicated impact of steam, hydrogen and oxygen pressure [29]. Therefore, incorporating co-dopants in CeO_2 could be a strategy for engineering WSR performance in SOECs.

Here, we perform computational studies on WSR on more candidate dopants, including Gd + Sb, Pr + Sb, Bi + Sb, Gd + Bi, and La + Bi trivalent pairs in CeO_2, as well as individual trivalent dopants such as Ga-, Sb-, Lu-, Gd-, Sm-, Pr-, Bi- and La-doped CeO_2, based on density-functional theory (DFT) [30]. This work will give more understanding of how cooperative dopants in ceria adjust the formation of reaction intermediates (especially the effect on the relative stability between dopant-H and Ce-H) and how they affect reaction kinetics of the WSR. We also investigated the effect of co-doping on oxygen diffusion and the effect of the relative position of trivalent pairs on the WSR activity. Our DFT works will give suggestions on how to choose a proper co-doped pair in ceria with good stability and excellent WSR activity.

2. Simulation models and methods

DFT studies are performed mainly on the WSR into H_2 via the hydridic H-species on the doped CeO_2(1 1 1) surface as illustrated in Fig. 1. As we have done in our previous studies on Gd doped CeO_2(1 1 1) [6], the computational model of individually doped and co-doped CeO_2(1 1 1) is built as a 2×3 surface unit cell consisting of three O-Ce-O atomic layers, with the O-Ce-O layer at the bottom fixed during all DFT studies. A vacuum gap with a thickness of 15 Å is applied in the unit cell to block the interaction between periodic cells. For creating doped CeO_2, two cerium atoms are substituted with two dopants (M1 and M2), as shown in Fig. 1, corresponding to doping concentration of 11%. When M1 = M2, we created individually doped CeO_2, including Ga-, Sb-, Lu-, Gd-, Sm-, Pr-, Bi-, and La-doped CeO_2. When M1 is different from M2, cooperative dopants in CeO_2 are created, such as Gd + Sb, Pr + Sb, Bi + Sb, Gd + Bi, and La + Bi co-doped CeO_2. As noted in Fig. 1, the studied M1 and M2 sit as nearest neighbors in the top layer of CeO_2(1 1 1), owing to the relatively higher stability compared to other relative positions (**Figure S1**) of M1 and M2, as shown in **Tables S1 and S2** in the supporting information. Our previous studies also found the favorable formation of trivalent dopants sitting as neighbors in the top layer of the ceria [28]. In addition to the good stability of trivalent pairs as neighbors in the top layer of the ceria surface, they also show excellent WSR performance. A more detailed discussion on the effect of the relative position of dopants on WSR is included in the section 'Results and discussions'.

To learn the structural properties of individually doped and co-doped ceria and their WSR performance, we conduct spin-polarized DFT calculations with the Perdew-Burke-Ernzerhof (PBE) [31] functional by using the Vienna ab initio simulation package (VASP, version 5.4.4) [32], where a Hubbard U term (U_{eff} = 4.5 eV [33–36]) is applied to the PBE functional to describe electron localization on the 4f shells of Ce, and Pr. No U corrections are applied to 4f shells of Gd, Sm, La, or Lu because we did not find any partial electron delocalization on them without a U correction. In addition, our previous studies have identified that the relative stability between dopant-H and Ce-H is not affected by the exact U_{eff} value [28]. U_{eff} = 4.5 eV is reasonable for investigating electrocatalysis on clean and doped CeO_2 [6,28]. The wave functions are expanded in plane waves with an energy cutoff of 550 eV [6,10] and a Γ-centered $3 \times 2 \times 1$ k-point mesh is used for sampling the Brillouin zone. The La($5d^16s^2$), Bi($4f^{14}5d^{10}6s^26p^3$), Lu($4f^{14}5d^16s^2$), Sb($4d^{10}5s^25p^3$), Ga($3d^{10}4s^24p^1$), Gd($4f^75d^16s^2$), Sm($4f^66s^2$), Pr($4f^36s^2$), and Ce($4f^15d^16s^2$) electrons were treated as valence states. The doped ceria surface is fully relaxed until reaching a force tolerance of 0.03 eV/Å. For La, Bi, Lu, Sb, and Ga, their spins have no initial setting because the magnetization is always zero when the valence equals + 3. For Gd, Sm and Ce, the initial setting of their spins did not affect identifying the final stable magnetization, as shown in **Tables S3-S5**, where the energy difference among different spin settings is smaller than 0.032 eV. However, among the studied cations, we found the final magnetization of Pr in Pr + Sb co-doped ceria is sensitive to the initial setting, as shown in **Table S6**, where the best initial guess of the spin of Pr^{3+} is 2, agreeing well with the previous studies [28]. The activation barriers of hydroxyl decomposition into H_2 in the individually doped and co-doped ceria are identified by the climbing image nudged-elastic band method [37] as implemented in VASP.

3. Results and discussions

As demonstrated in our previous studies, H_2 production on partially hydroxylated ceria needs to overcome a high barrier of 3.0–3.5 eV [6,12]. Instead, it is usually more favorable to form more hydroxyls on ceria by creating more oxygen vacancies and further via water dissociation, finally leading to the WSR proceeding readily on an overly hydroxylated ceria surface through a barrier below 3.0 eV (2.2 eV for Gd doped ceria [6], and 1.7 eV for Pr + Bi co-doped ceria [28]). On the studied ceria surface, 6H bind with lattice oxygen to form the fully hydroxylated ceria. There are two stable configurations for the formation of an overly hydroxylated surface (7H). One possibility is that the seventh H binds with one lattice oxygen in the subsurface. The other possibility is that the seventh H binds with trivalent metal to form hydridic H (dopant-H or Ce-H), as shown in **Figure S2**. Herein, WSR pathways via the formation

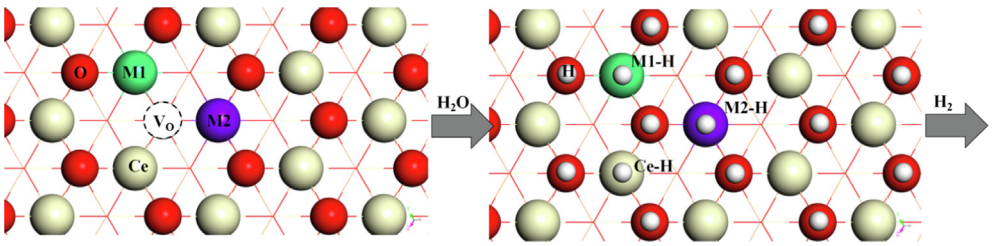

Fig. 1. The illustrated WSR into H_2 on the doped CeO_2(1 1 1) surface, where H_2O easily dissociates into Ce-H, M1-H, M2-H hydridic H moieties on the doped surface. V_O is an oxygen vacancy, while M1 and M2 are two trivalent dopants. The atoms in the deep layers are displayed as lines.

of 6H, dopant-H (M1-H or M2-H), and Ce-H are systematically investigated on differently doped ceria. The corresponding reaction steps are illustrated in **Figure S2**, where the net reaction is $H_2O \rightarrow H_2 + 1/2O_2$, and reactions along different reaction pathways are described below **Figure S2**. The identified stable dopant-H and Ce-H configurations are presented in **Figures S3-S5**. The top and side views of M−H (Ce-H or dopant-H) in Gd + Sb co-doped ceria labeled with M−H bond lengths are presented in **Figure S5**. M−H bond lengths of other doped ceria are listed in **Table S7**, where the bond length of Ce-H in doped ceria is around 2.3 Å and the bond length of Sb-H in Gd + Sb, Bi + Sb, and Pr + Sb co-doped ceria is as low as 1.7 Å, indicating the stable formation of hydridic H-species in co-doped ceria. For the reaction on the clean ceria, $2Ce^{3+}$ are oxidized to $2Ce^{4+}$ due to the formation of Ce-H ($Ce^{4+}H^-$) on clean ceria via the reaction $7H^+ + 7Ce^{3+} \rightarrow 6H^+ + 5Ce^{3+} + Ce^{4+} + Ce^{4+}H^-$, where the formal oxidation states are induced from the atomic spin states. The oxidation of $2Ce^{3+}$ to $2Ce^{4+}$ is also found in the doped ceria because of the formation of dopant-H (M1-H or M2-H) via the reaction of $7H^+ + 5Ce^{3+} + M1^{3+} + M2^{3+} \rightarrow 6H^+ + 3Ce^{3+} + 2Ce^{4+} + M1^{3+} + M2^{3+}H^-$, with the exception of the formation of Sb-H on Sb, Gd + Sb, Pr + Sb, and Bi + Sb doped ceria, where $Sb^{5+}H^-$ forms via the reaction of $7H^+ + 5Ce^{3+} + Sb^{3+} + M^{3+} \rightarrow 6H^+ + 5Ce^{3+} + M^{3+} + Sb^{5+}H^-$ (M = Sb, Gd, Pr, or Bi). Thus, for the formation of hydridic H-species including dopant-H and Ce-H, it is $Ce^{4+}H^-$ for Ce-H, $Sb^{5+}H^-$ for Sb-H, while for other trivalent dopants it is $M^{3+}H^-$.

Fig. 2 and S6-S15 show the free energy diagrams of WSR on individually doped or co-doped CeO_2(1 1 1) via the formation of 6H, dopant-H, and Ce-H at 800 K (an intermediate operation temperature of SOECs [2]). The free energy diagrams of the WSR on Gd-, Pr-, and Bi-doped ceria have been shown in our previous works [6,28], and thus are not presented in the supporting information. The free energy of reaction intermediates is calculated relative to the clean ceria surface by assuming the ceria-gas interface equilibrium with water steam and H_2 at 1 bar pressure and 800 K, referring to our previous DFT studies for more calculation details [6,10]. For producing one H_2 molecule, the breaking of the first O–H bond is difficult, and the highest transition states (TS) are associated with this bond breaking, as shown in Fig. 2 and S6-S15. Fig. 2 is a simplified reaction diagram and shows reactions via 5H + V_O, 6H, Ce-H and Sb-H. A full reaction pathway of WSR on Gd-Sb co-doped ceria is shown in **Figure S6**, where the barrier for producing one H_2 is 3.9, 3.5, 3.2, and 3.3 via 2H, 4H, 5H + V_O, and 6H, respectively. However, H_2 is produced easily via the formation of an hydridic-H intermediate, through a 1.7 eV barrier via the Ce-H. For the H_2 production via 7H → Sb-H → H_2, a 1.5 eV barrier is firstly required for the formation of Sb-H. Then the decomposition of Sb-H involves the reaction between Sb-H and one O–H nearest to Sb, as presented in Fig. 2, leading to a 1.1 eV barrier for releasing one H_2 molecule. Both reaction barriers occurring before and after Sb-H are lower compared to the WSR via other paths, making the most efficient reaction pathway proceeding via the Sb-H on Gd + Sb co-doped ceria. In addition, a full reaction path in **Figure S6** shows lower free energy of high H coverage like 5H, 6H, and 7H compared to the formation of 2H, indicating the facile formation of high H coverage at 800 K. It is found that for the WSR on Lu-, Sm-individually doped CeO_2(1 1 1), the most efficient reaction pathway is that the WSR proceeds via the formation of Ce-H, where the free energy of Ce-H is lower than dopant-H, as shown in **Figures S7-S10**. When it forms Gd + Sb, Pr + Sb, Bi + Sb pairs in CeO_2(1 1 1), the favorable reaction pathway shifts to that via the formation of dopant-H, where dopant-H becomes 1.0 eV more stable than Ce-H in Gd + Sb, as shown in **Figure 2**, and 1.3 eV more stable than Ce-H in Bi + Sb or Pr + Sb co-doped ceria, as noted in **Figures S14 and S15**. Our DFT calculations found that the improved stability of dopant-H by co-doping leads to more facile H_2 production via the formation of dopant-H than that via Ce-H.

To evaluate oxygen diffusion in doped ceria, the nearest-neighbor oxygen vacancy to dopants is investigated as illustrated in **Figure S16** because creating one oxygen vacancy near the dopants is reported more stable than other positions [6,28]. **Table S8** shows the formation energy of one oxygen vacancy in the subsurface and that in the top surface of doped CeO_2(1 1 1), and its diffusion barrier from the subsurface to the top surface (diffusion paths are presented in **Figure S17**), where the data of Gd-doped ceria and pure ceria is taken from our previous work [6]. The formation energy of one oxygen vacancy in the studied doped CeO_2(1 1 1) is within 1.50 eV. However, it increases to 2.18 eV in the pure CeO_2(1 1 1), as shown in **Table S8**, suggesting a much more favorable formation of oxygen vacancy in doped ceria than pure ceria. The identified diffusion barriers of one oxygen vacancy in individually doped ceria are comparable to the previously reported data [38–40]. As noted in **Table S8**, a smaller diffusion barrier (ranging from 0.09 to 0.66 eV) is found in co-doped ceria compared to the individually doped ceria (ranging from 0.17 to 0.80 eV). When the surface is covered by 5H, the diffusion barrier in Gd + Sb co-doped ceria remains lower than that in Gd-doped ceria, as shown in **Figure S18**. Therefore, our studies suggest an improved oxygen diffusion in ceria-based SOECs by co-doping.

Then, the WSR performance of differently doped ceria is evaluated by comparing the turn-over frequency (TOF) toward H_2 production, which is calculated using the energetic span (δE) [41,42] between TOF determining intermediate and TOF determining transition state. In Fig. 2, the TS for producing one H_2 via Sb-H is the TOF determining transition state (TDTS), and 5H + V_O^{sur} with the lowest free energy is the TOF determining intermediate (TDI). TOF is calculated by the equation.

$$TOF = \frac{k_B T}{h} \exp\left(\frac{-\delta E}{k_B T}\right)$$

It has been found that the TDTS is always associated with producing one H_2 via hydridic H-species (Ce-H or dopant-H), as noted in Fig. 2 and S7-S15, where 6H or 5H + V_O before the formation of hydridic H-species is identified as the TDI. It indicates that TDI and TDTS occur before and after the hydridic H-species, respectively, making hydridic H-species the key intermediates during WSR on doped ceria.

In addition to the WSR performance, the stability of incorporating ceria with dopants is evaluated by the doping energy (E_f), which is the energy required to substitute one cerium oxide (CeO_2) with trivalent metal oxide ($M1_2O_3$ or $M2_2O_3$) and is defined as.

$$2E_f = E[M1M2Ce_{x-2}O_{2x-1}] - E[Ce_xO_{2x}] - 0.5 \times E[M1_2O_3] - 0.5 \times E[M2_2O_3] + 2 \times E[CeO_2].$$

Fig. 3 (a) presents the calculated doping energy, and the calculated TOF toward H_2 production on differently doped ceria at 800 K is shown in Fig. 3 (b). The studied TOF in Fig. 3 is in the form of Log (TOF), suggesting a linear relationship between Log (TOF) and the energetic span (δE) according to the formula of $TOF = \frac{k_B T}{h} \exp\left(\frac{-\delta E}{k_B T}\right)$. TOF is found to correlate well with the average radius of the studied trivalent cations, where TOF decreases with an increasing average radius of trivalent cations and Gd + Sb, Pr + Sb, and Bi + Sb trivalent pairs show superior performance with TOF 2–4 orders of magnitude larger than individually doped ceria such as Ga-, Sb-, Lu-, Gd-, Sm-, Pr-, Bi- and La-doped CeO_2. It is noted from Fig. 3 (b) that the trivalent dopants with small radius like Ga^{3+}, Sb^{3+}, and Lu^{3+} are not included in the correlation because of larger doping energy than other dopants, as shown in Fig. 3 (a). Larger doping energy in Ga-, Sb- and Lu-doped ceria suggests instability of ceria incorporated with individual Ga, Sb, or Lu. Therefore,

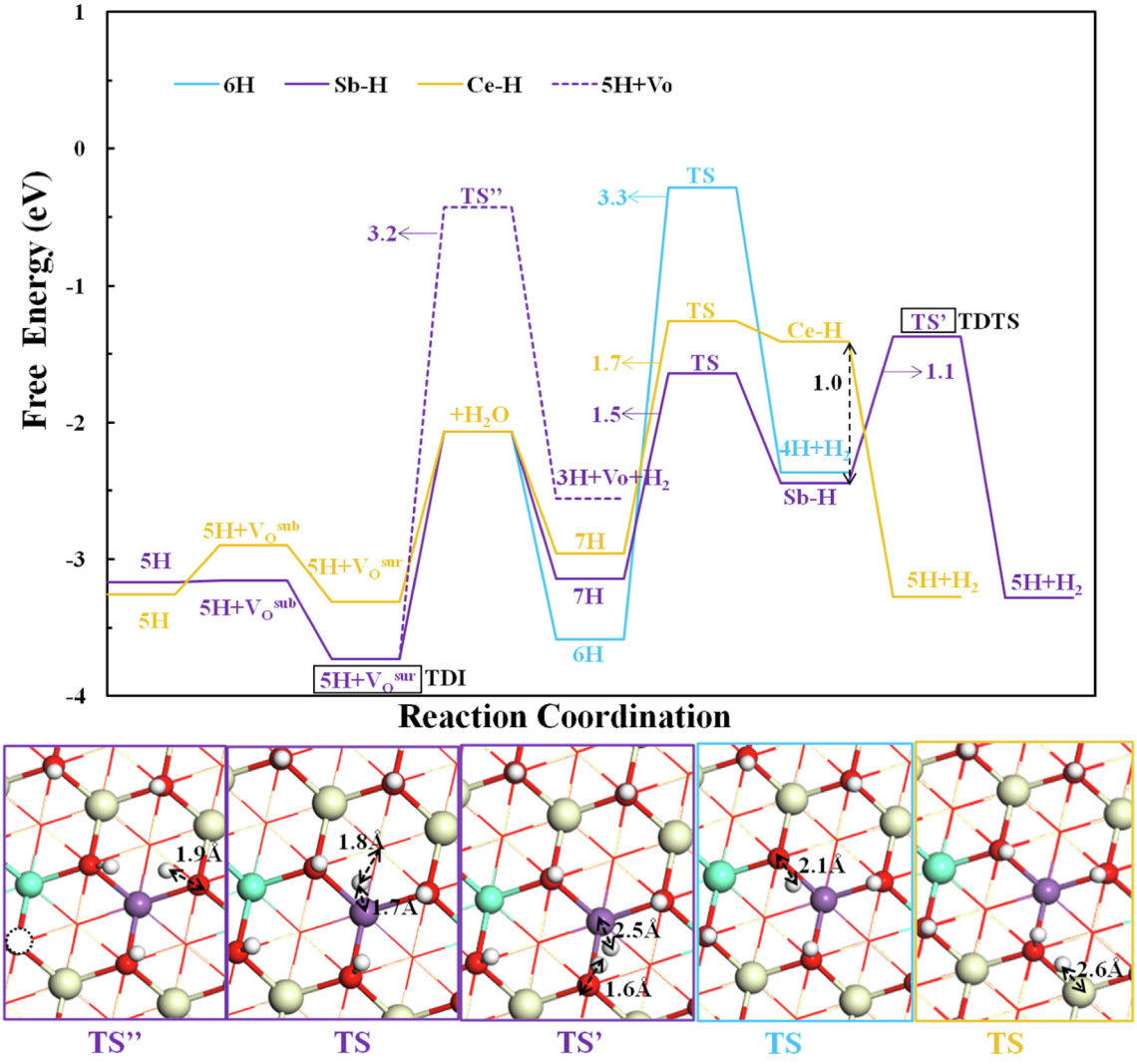

Fig. 2. Reaction pathways of the WSR on Gd + Sb co-doped CeO_2(1 1 1) via the formation of 6H, 5H + V_O, Sb-H, and Ce-H at 800 K, where Sb-H is 1.0 eV more stable than Ce-H. Transition states (TS) are presented at the bottom.

Ga-, Sb-, and Lu-doped ceria are not included in the following discussions. The TOF of the WSR on individual dopants like Pr, and Bi that have an ionic radius close to Ce, is comparable to clean ceria. However, the WSR activity is enhanced significantly through the cooperative Pr + Sb, and Bi + Sb co-doping, suggesting a synergistic effect of co-doping in CeO_2 for promoting WSR. In addition to the excellent WSR performance on co-doped ceria, Fig. 3 (a) shows good stability of co-dopants in ceria due to low doping energy. Therefore, our DFT studies suggest that incorporating ceria with co-dopants, like Gd + Sb, Pr + Sb, and Bi + Sb, is an effective strategy for promoting WSR on ceria-based cathodes in SOECs.

We have investigated the effect of potential on the free energy at each step of WSR on Gd + Sb co-doped ceria, as shown in **Figure S19** and found the TS for producing one H_2 via Sb-H remains the TDTS under the potential of −0.2 V. At the same time, 5H + V_O with the lowest free energy remains the TDI. The free energy change for the formation of the TDI from the 5H surface at −0.2 V is 0.4 eV lower compared to that at zero potential because introducing the oxygen vacancy becomes more facile at more reducing potentials. This leaves the energetic span for the WSR unaffected by the applied potential, whereas the energetic span for the reverse hydrogen oxidation reaction increases by 0.4 eV. For the WSR on doped ceria at −0.2 V, the TDTS is always associated with producing one H_2 via hydridic H-species (Ce-H or dopant-H), while 6H or 5H + V_O before the formation of hydridic H-species is identified as the TDI, as noted in **Figures S7-S15 and S19**, in line with the findings at zero potential. **Figure S20** shows a correlation between TOF and ionic radius at −0.2 V, where Gd + Sb, Pr + Sb, and Bi + Sb with smaller ionic radius hold higher WSR activity than other dopants, in line with the findings at zero potential, as shown in Fig. 3. Therefore, the improvement in WSR activity by co-doping is not affected by applying a potential of −0.2 V.

We also investigated the effect of the relative position of trivalent co-dopants on the WSR activity. For the individually doped and co-doped CeO_2, two dopants sitting as nearest neighbors in the top layer is found to be more stable than other relative position, as noted in **Tables S1 and S2**, except Gd-, Sb-, Gd + Sb doped ceria. The energy of two dopant neighbors, with one located in the subsurface, is comparable to that two dopants sit on the top surface in Gd-doped ceria. At the same time, it becomes 0.454 eV more stable when two dopants sit on the top surface in Sb-doped ceria, as shown in **Table S2**. In Gd-doped ceria, WSR on the surface that 2Gd are neighbors with one Gd located in the subsurface is investigated because of the more favorable formation of hydroxyls than other relative positions of 2Gd, which has been detailedly discussed in our previous work [6]. In Sb-doped ceria, the WSR on the surface with 2Sb neighbors and one located in the subsurface

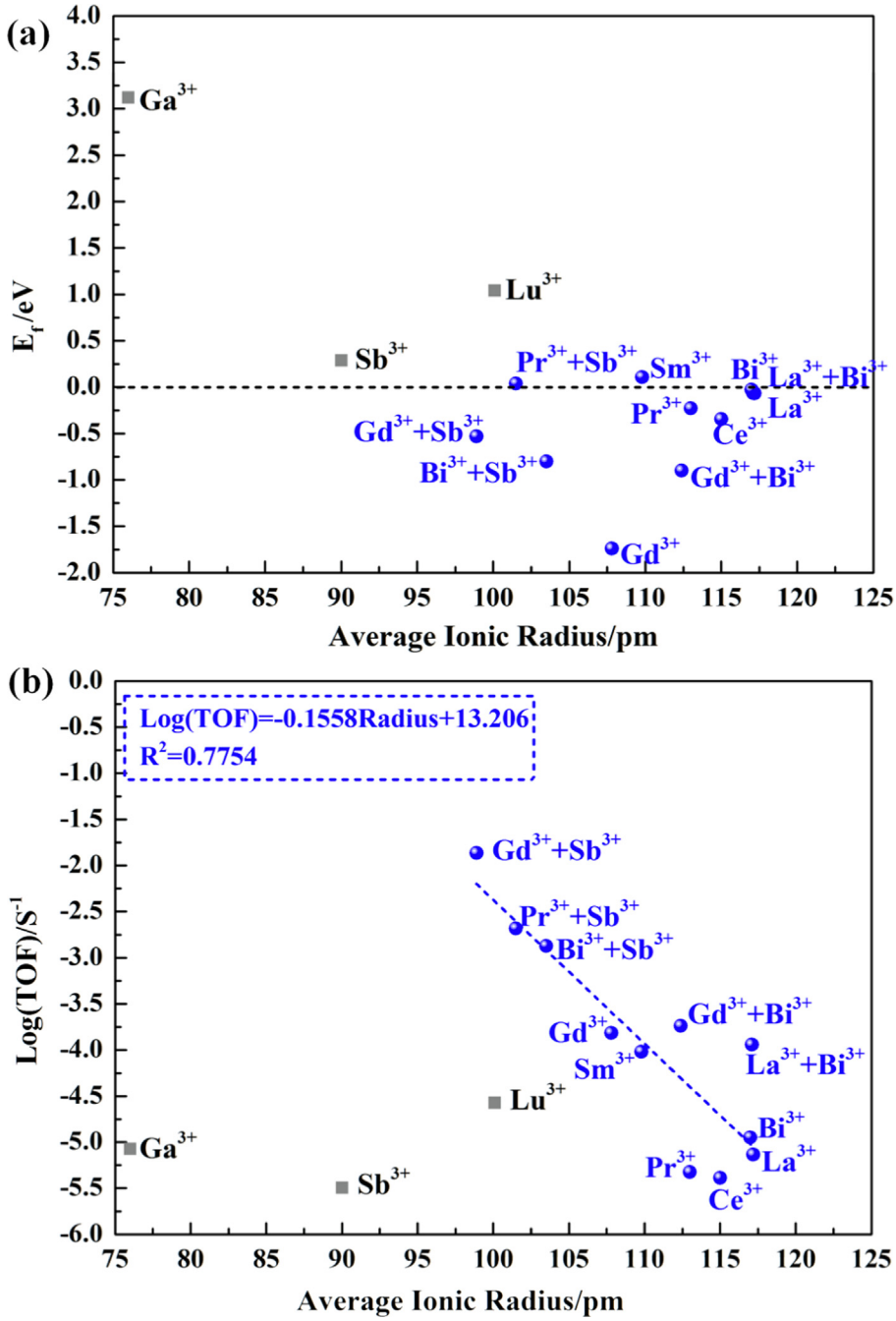

Fig. 3. **(a)** Comparison of the doping energy of individually doped and co-doped CeO_2. **(b)** The correlation between the turn-over frequency (TOF) of producing H_2 at 800 K and the average radius of the studied trivalent dopants.

is not further addressed because the doping energy is 1.28 eV higher than that 2Sb sitting on the top surface.

However, for Gd + Sb pairs, we found similar energy (within 0.02 eV) when Gd and Sb are nearest neighbors with Gd in the sublayer and when they are next-nearest neighbors with Gd in the sublayer. Then, more DFT calculations are conducted to investigate the effect of the relative position of Gd + Sb pairs on the WSR. The calculated reaction pathways are shown in **Figure S21**, where the formation of the surface that Sb sitting in the sublayer is found to be 0.8–1.1 eV unstable, and the formation of dopant-H is unfavorable compared to other relative positions, agreeing well with our previous findings that more favorable formation of reaction intermediates on a stable surface [28]. Although the free energy of Sb-H is comparable on the surfaces that Sb sits on the top surface, we found much more stable 6H, 7H, and 5H + H_2 on the Gd + Sb pair when Gd and Sb are exposed as nearest neighbors in the top surface and also much lower reaction barrier for H_2 production compared to the other relative positions (1.1 eV barrier for the Gd + Sb pair sitting as neighbors in the top layer, while 1.6 eV barrier for the pair that is not neighbored, as shown in **Figure S21**). Therefore, our DFT studies show that trivalent pairs sitting as neighbors in the studied ceria surface have better WSR performance than other relative positions.

The above superior WSR performance on Gd + Sb, Pr + Sb, and Bi + Sb trivalent pairs compared to other doped ceria is attributed to the much more favorable formation of dopant-H over Ce-H as

presented in Fig. 4 (a) and **Table S9**, where the formation energy of dopant-H is 2.5–3.0 times lower than Ce-H on Gd + Sb, Pr + Sb, and Bi + Sb co-doped ceria. At the same time, it is comparable to Ce-H on other doped ceria. Lower energy in Fig. 4 suggests a more stable formation in DFT studies. In Fig. 4, Ga-, Sb-, and Lu-doped ceria are marked in grey and are not included in the discussion because of low stability, as found in Fig. 3 (a). The more favorable formation of Sb-H over Ce-H in Gd + Sb, Pr + Sb, and Bi + Sb co-doped ceria introduces two more electrons that localize on the 4f orbitals of Ce, finally leading to the formation of $5Ce^{3+}$ for Sb-H binding, while only $3Ce^{3+}$ form for Ce-H binding, as noted in **Figures S4 and S5**. Therefore, the strong Sb-H binding in doped ceria shows donor-type conducting behavior, corresponding to the shift of E_f close to the conductive band for Sb-H binding compared to Ce-H binding, as shown in **Figures S22-S24.** The donor-type conducting behavior for Sb doped ceria has also been observed experimentally [27]. However, we did not identify a significant difference between the shift of E_f in other doped ceria (**Figure S25-S35**).

In addition, we find a linear correlation between the ionic radius of the studied dopants and the formation energy of the most stable hydridic H moiety on each doped-ceria surface, as shown in Fig. 4 (b), suggesting that incorporating ceria with small trivalent pairs that have an average radius close to Gd + Sb, Pr + Sb or Bi + Sb can significantly improve the formation of the dopant-H. The more favorable formation of dopant-H over Ce-H leads to facile H_2 production via dopant-H, further enhancing the WSR performance on ceria, as shown in **Figures 3, S14 and S15**. At the same time, La + Bi and Gd + Bi co-dopants in ceria do not improve the WSR activity as significantly as Gd + Sb, Pr + Sb or Bi + Sb co-dopants, which is explained by the comparable formation energy of the hydridic H moiety on La-, Bi-, Gd- individually doped and co-doped ceria as noted in Fig. 4 **(b)**.

The ionic radius of dopants has often been used to evaluate lattice parameters of the doped CeO_2 [43], the stability of creating oxygen vacancies [44], reduction energy [45], binding energies of oxygen vacancies and dopants [46], kinetic barriers of oxygen diffusion in doped CeO_2 [44,47] and catalysis on doped ceria [48]. We have found a correlation between the energetic span (δE) and ionic radius and a correlation between the energetic span (δE) and E (Metal-H), as shown in **Figure S36**, which means the calculated energetic span (δE) for WSR via hydridic H-species (Ce-H or dopant-H) is dependent on the energy of hydridic H-species. Log (TOF) is also well described by the oxygen diffusion barrier, as shown in **Figure S37**, where oxygen diffusion barriers correlate with the radius of dopants, as shown in **Figure S38**. A decreased barrier in ceria incorporated with small dopants is understood because the small dopants enable more space for oxygen diffusion, indicating faster ionic conductivity in SOECs and facile formation of more oxygen vacancies in ceria surfaces (high reducibility of ceria) that further enables the formation of hydridic H-species via water dissociation.

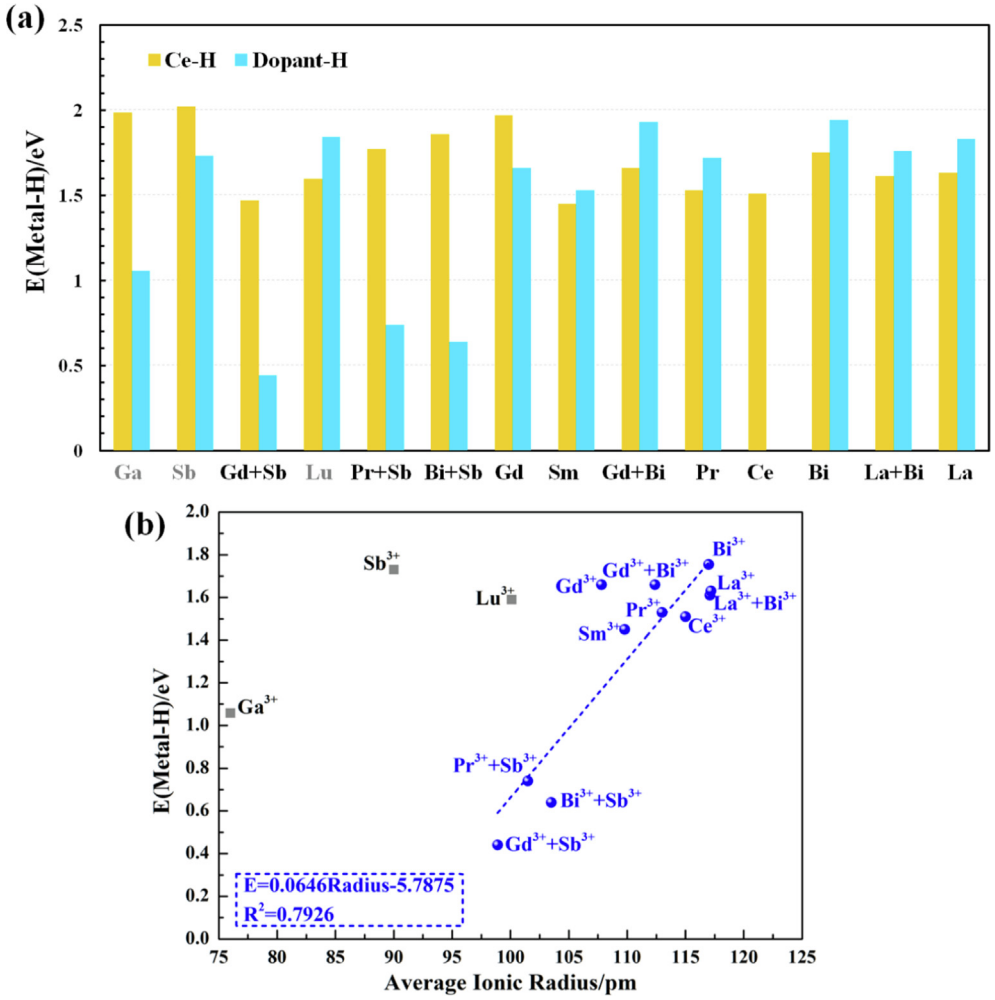

Fig. 4. **(a)** The formation energy of the Ce-H and dopant-H on doped ceria surfaces. **(b)** The linear correlation between the average dopant radius and the formation energy of the most stable hydridic H intermediate, E(Metal-H).

In addition to the improved relative stability of dopant-H over Ce-H by Gd + Sb, Pr + Sb or Bi + Sb co-doping, surface local strain induced by co-doping could also contribute to the enhanced WSR activity on Gd + Sb, Pr + Sb or Bi + Sb co-doped ceria. Our previous work has shown that applying tensile strain can stabilize the formation of hydridic H-species on pure CeO_2(1 1 1) [10]. Therefore, incorporating ceria with small co-dopants such as Gd + Sb, Pr + Sb or Bi + Sb with 13% radius mismatch to pure ceria can achieve a large tensile strain, which could facilitate the formation of hydridic H-species, in line with a small E(Metal-H) for Gd + Sb, Pr + Sb, and Bi + Sb co-doped ceria, as noted in Fig. 4**(a)**.

SOECs usually operate at a temperature around 1200 K [1,2,4]. We further compare the WSR activity at operating temperatures ranging from 400 to 1200 K, as presented in Fig. 5. The corresponding energetic span for H_2 production at different temperature is listed in **Table S10**. For individually doped ceria, Gd- and Sm-doped ceria holds better WSR performance than Pr-, Bi-, and La-doped ceria, as noted in Fig. 5. Adding Gd or La into Bi-doped ceria that leads to the formation of Gd + Bi, La + Bi co-doped pairs can improve the TOF toward H_2 production as high as that on Gd- and Sm-doped ceria. The reported operation temperature on Gd-doped ceria can be extended to 773–1073 K [49,50]. To reach the same TOF on Gd-doped ceria at 773–1073 K, the operating temperature can be extended to 600–1000 K (as shown in Fig. 5) by incorporating ceria with the Gd + Sb pair and extended to 700–1000 K in Pr + Sb, Bi + Sb co-doped ceria, indicating that Gd + Sb, Bi + Sb, and Pr + Sb co-doping in ceria allows WSR at an intermediate temperature below 1000 K. TOF of the WSR on Gd + Sb is 10 times higher than Gd-doped ceria at 1000 K, 10^2 times higher than Gd-doped ceria at 800 K, and is up to 10^5 times higher than Gd-doped ceria at 600 K, showing excellent WSR performance on co-doped ceria at an intermediate temperature below 1000 K.

4. Conclusions

By performing DFT studies of H_2 production via the WSR on individually Ga-, Sb-, Lu-, Gd-, Sm-, Pr-, Bi- and La-doped CeO_2, as well as Gd + Sb, Pr + Sb, Bi + Sb, Gd + Bi, and La + Bi co-doped CeO_2, we find the stability of the key intermediates, hydridic H-species (dopant-H or Ce-H), is substantially improved by incorporating ceria with Gd + Sb, Pr + Sb, and Bi + Sb pairs, where dopant-H becomes much more stable than Ce-H, leading to WSR proceeding more readily via dopant-H than Ce-H. The energy of hydridic H-species and the turn-over frequency toward H_2 production are found to correlate well with the average radius of paired trivalent cations. A correlation between TOF and ionic radius at −0.2 V is also found. In addition, the effect of the relative position of dopants on WSR was investigated, showing that trivalent pairs sitting as neighbors in the studied ceria surface have better WSR performance than the pairs far away from each other. DFT calculations also observe an improved oxygen diffusion in ceria-based SOECs by co-doping. TOF is also well described by the oxygen diffusion barrier. We further found that Gd + Sb, Pr + Sb, and Bi + Sb co-doped ceria allow WSR at an intermediate temperature below 1000 K and hold superior WSR performance with TOF 2–5 orders of magnitude larger than individual trivalent dopants. Therefore, our DFT studies propose cooperative trivalent pairs as an effective strategy for improving the WSR on CeO_2 in SOECs and suggest proper candidates such as Gd + Sb, Pr + Sb, Bi + Sb, or the pairs with an average radius close to these.

Data availability

Data will be made available on request.

Declaration of Competing Interest

The authors declare that they have no known competing financial interests or personal relationships that could have appeared to influence the work reported in this paper.

Acknowledgments

This work was financially supported by the Velux Foundations through the research center V-Sustain (grant number 9455), natural science program on basic research project of Shaanxi province (2023-JC-QN-0155), and the Qinchuangyuan project of Shaanxi province (QCYRCXM-2022-31). The partial simulations on the effect of the relative position of dopants on WSR performance were conducted on supercomputing facilities provided by Hefei Advanced.

Appendix A. Supplementary material

Supporting data includes figures of free energy diagrams, atomic configurations, and density of states, and supporting tables of energy of dopants with different relative positions, the formation energy of Ce-H and dopant-H on doped ceria, energetic span for H_2 production on stoichiometric and doped CeO_2(1 1 1), the oxygen formation energy and diffusion barrier, and other correlations. The supporting information is available free of charge and can be found online at Journal of Catalysis. Supplementary data

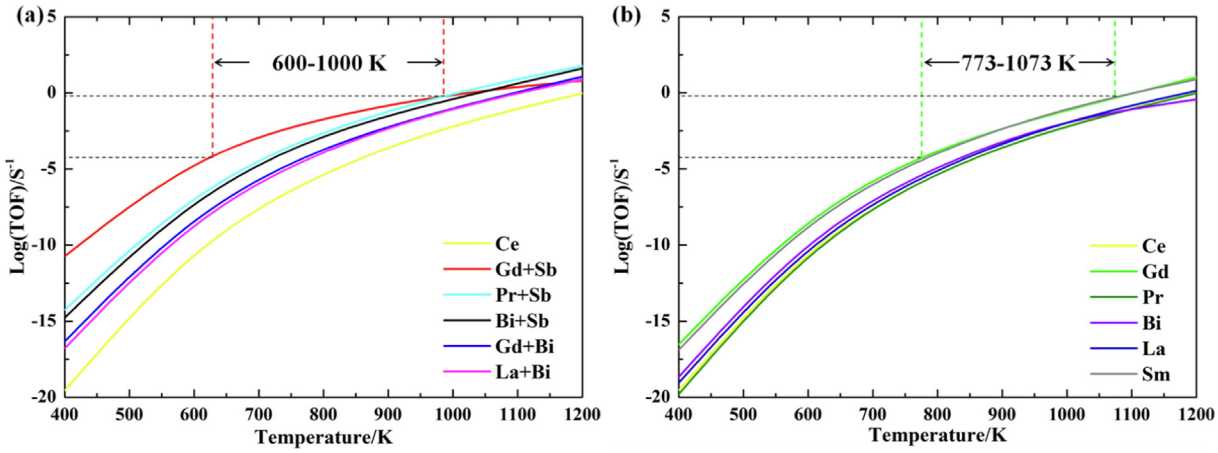

Fig. 5. The TOF of producing H_2 over the (a) co-doped and (b) individually doped ceria is a function of reaction temperature.

to this article can be found online at https://doi.org/10.1016/j.jcat.2023.02.010.

References

[1] F.M. Sapountzi, J.M. Gracia, C.J. Weststrate, H.O.A. Fredriksson, J.W. Niemantsverdriet, Electrocatalysts for the generation of hydrogen, oxygen and synthesis gas, Prog. Energy Combust. Sci. 58 (2017) 1–35.

[2] J.T.S. Irvine, D. Neagu, M.C. Verbraeken, C. Chatzichristodoulou, C. Graves, M.B. Mogensen, Evolution of the electrochemical interface in high-temperature fuel cells and electrolysers, Nat. Energy. 1 (2016) 15014.

[3] Z.A. Feng, F. El Gabaly, X. Ye, Z.-X. Shen, W.C. Chueh, Fast vacancy-mediated oxygen ion incorporation across the ceria–gas electrochemical interface, Nat. Commun. 5 (2014) 4374.

[4] A. Brisse, J. Schefold, M. Zahid, High temperature water electrolysis in solid oxide cells, Int. J. Hydrogen Energy. 33 (2008) 5375–5382.

[5] J. Chi, H. Yu, Water electrolysis based on renewable energy for hydrogen production, Chinese, J. Catal. 39 (2018) 390–394.

[6] T. Wu, Q. Deng, H.A. Hansen, T. Vegge, Mechanism of water splitting on gadolinium-doped C_eO2(111): A DFT+U study, J. Phys. Chem. C. 123 (2019) 5507–5517.

[7] X. Tong, S. Ovtar, K. Brodersen, P.V. Hendriksen, M. Chen, A 4 × 4 cm^2 nanoengineered solid oxide electrolysis cell for efficient and durable hydrogen production, ACS Appl. Mater. Interfaces. 11 (2019) 25996–26004.

[8] H.A. Hansen, C. Wolverton, Kinetics and thermodynamics of H_2O dissociation on reduced CeO_2(111), J. Phys. Chem. C. 118 (2014) 27402–27414.

[9] M. Molinari, S.C. Parker, D.C. Sayle, M.S. Islam, Water adsorption and its effect on the stability of low index stoichiometric and reduced surfaces of ceria, J. Phys. Chem. C. 116 (2012) 7073–7082.

[10] T. Wu, T. Vegge, H.A. Hansen, Improved electrocatalytic water splitting reaction on CeO_2(111) by strain engineering: A DFT+*U* study, ACS Catal. 9 (2019) 4853–4861.

[11] Z. Yang, Q. Wang, S. Wei, D. Ma, Q. Sun, The effect of environment on the reaction of water on the ceria (111) surface: A DFT+*U* study, J. Phys. Chem. C. 114 (2010) 14891–14899.

[12] T. Wu, N. López, T. Vegge, H.A. Hansen, Facet-dependent electrocatalytic water splitting reaction on CeO_2: A DFT+*U* Study, J. Catal. 388 (2020) 1–10.

[13] L. Gill, A. Beste, B. Chen, M. Li, A.K.P. Mann, S.H. Overbury, E.W. Hagaman, Fast MAS ^{1}HNMR study of water adsorption and dissociation on the (100) surface of ceria nanocubes: A fully hydroxylated, hydrophobic ceria surface, J. Phys. Chem. C. 121 (2017) 7450–7465.

[14] F. Dvořák, L. Szabová, V. Johánek, M. Farnesi Camellone, V. Stetsovych, M. Vorokhta, A. Tovt, T. Skála, I. Matolínová, Y. Tateyama, J. Mysliveček, S. Fabris, V. Matolín, Bulk hydroxylation and effective water splitting by highly reduced cerium oxide: The role of O vacancy coordination, ACS Catal. 8 (2018) 4354–4363.

[15] Z. Wu, Y. Cheng, F. Tao, L. Daemen, G.S. Foo, L. Nguyen, X. Zhang, A. Beste, A.J. Ramirez-Cuesta, Direct neutron spectroscopy observation of cerium hydride species on a cerium oxide catalyst, J. Am. Chem. Soc. 139 (2017) 9721–9727.

[16] Y. Park, S.K. Kim, D. Pradhan, Y. Sohn, Surface treatment effects on CO oxidation reactions over Co, Cu, and Ni-doped and codoped CeO_2 catalysts, Chem. Eng. J. 250 (2014) 25–34.

[17] Z. Pu, X. Liu, A. Jia, Y. Xie, J. Lu, M. Luo, Enhanced activity for CO oxidation over Pr- and Cu-doped CeO_2 Catalysts: Effect of oxygen vacancies, J. Phys. Chem. C. 112 (2008) 15045–15051.

[18] S. Banerjee, P.S. Devi, D. Topwal, S. Mandal, Enhanced ionic conductivity in $Ce_{0.8}Sm_{0.2}O_{1.9}$: Unique effect of calcium co-doping, Adv. Funct. Mater. 17 (2007) 2847–2854.

[19] Y. Dong, S. Hampshire, B. Lin, Y. Ling, X. Zhang, High sintering activity Cu–Gd co-doped CeO_2 electrolyte for solid oxide fuel cells, J. Power Sources. 195 (2010) 6510–6515.

[20] G. Zhou, W. Xiao, W. Geng, J. Wang, B. Xue, L. Wang, Improvement of the homogeneity and oxygen storage capability of Ce_{1-x} $Zr_xO_{2-\delta}$ by co-doping: A first-principles study, J. Alloys Compd. 817 (2020).

[21] K. Sandhya, N.S. Chitra Priya, D.N. Rajendran, P. Thappily, Structural and electrical properties of cerium oxides doped by Sb^{3+} and Bi^{3+} cations, J. Electron. Mater. 49 (2020) 4936–4944.

[22] R. Farra, M. García-Melchor, M. Eichelbaum, M. Hashagen, W. Frandsen, J. Allan, F. Girgsdies, L. Szentmiklósi, N. López, D. Teschner, Promoted ceria: A structural, catalytic, and computational study, ACS Catal. 3 (2013) 2256–2268.

[23] H. Inaba, R. Sagawa, H. Hayashi, K. Kawamura, Molecular dynamics simulation of gadolinia-doped ceria, Solid State Ionics. 122 (1999) 95–103.

[24] X. Aparicio-Anglès, A. Roldan, N.H. De Leeuw, Gadolinium-vacancy clusters in the (111) surface of gadolinium-doped ceria: A density functional theory study, Chem. Mater. 27 (2015) 7910–7917.

[25] D.E.P. Vanpoucke, P. Bultinck, S. Cottenier, V. Van Speybroeck, I. Van Driessche, Aliovalent doping of CeO_2: DFT study of oxidation state and vacancy effects, J. Mater. Chem. A. 2 (2014) 13723–13737.

[26] T. Kolodiazhnyi, T. Charoonsuk, M. Spreitzer, N. Vittayakorn, Analysis of Sb-doped ceria: Magnetism, conductivity, dielectric, specific heat and optical properties, J. Eur. Ceram. Soc. 39 (2019) 418–423.

[27] K. Neuhaus, B. Gerke, O. Niehaus, S. Koops, T. Hopp, R. Pöttgen, H.-D. Wiemhöfer, Investigation of the cation valency and conductivity of antimony-substituted ceria, J. Solid State Electrochem. 20 (2016) 2295–2304.

[28] T. Wu, T. Vegge, H.A. Hansen, Enhanced activity for electrocatalytic H_2 production through cooperative Pr and Bi co-doping of CeO_2 in solid oxide electrolysis cells, J. Catal. 402 (2021) 310–314.

[29] N. Mazzanti, Ceria-based thin film electrodes for sustainable hydrogen production, Kgs. Lyngby: DTU Energy, 2021. 256 p.

[30] R.G. Parr, Density functional theory, Ann. Rev. Phys. Chern. 34 (1983) 631–656.

[31] J.P. Perdew, K. Burke, M. Ernzerhof, Generalized gradient approximation made simple, Phys. Rev. Lett. 77 (1996) 3865–3868.

[32] G. Kresse, J. Furthmüller, Efficient iterative schemes for ab initio total-energy calculations using a plane-wave basis set, Phys. Rev. B. 54 (1996) 11169–11186.

[33] M. Capdevila-Cortada, M. García-Melchor, N. López, Unraveling the structure sensitivity in methanol conversion on CeO_2: A DFT+*U* study, J. Catal. 327 (2015) 58–64.

[34] Y.Q. Su, I.A.W. Filot, J.X. Liu, I. Tranca, E.J.M. Hensen, Charge transport over the defective CeO_2(111) surface, Chem. Mater. 28 (2016) 5652–5658.

[35] S. Fabris, S.D. Gironcoli, S. Baroni, G. Vicario, G. Balducci, Reply to Comment on "Taming multiple valency with density functionals: A case study of defective ceria", Phys. Rev. B. 72 (2005).

[36] K. Michel, T.S. Bjørheim, T. Norby, J. Janek, M.T. Elm, Importance of the spin-orbit interaction for a consistent theoretical description of small polarons in Pr-doped CeO_2, J. Phys. Chem. C. 124 (2020) 15831–15838.

[37] G. Henkelman, B.P. Uberuaga, H. Jónsson, Climbing image nudged elastic band method for finding saddle points and minimum energy paths, J. Chem. Phys. 113 (2000) 9901–9904.

[38] H.-T. Chen, J.-G. Chang, H.-L. Chen, S.-P. Ju, Identifying the O_2 diffusion and reduction mechanisms on CeO_2 electrolyte in solid oxide fuel cells: A DFT+*U* study, J. Comput. Chem. 30 (2009) 2433–2442.

[39] D.A. Andersson, S.I. Simak, N.V. Skorodumova, I.A. Abrikosov, B. Johansson, Optimization of ionic conductivity in doped ceria, PNAS. 103 (2006) 3518–3521.

[40] P.P. Dholabhai, J.B. Adams, P. Crozier, R. Sharma, Oxygen vacancy migration in ceria and Pr-doped ceria: A DFT+*U* study, J. Chem. Phys. 132 (2010).

[41] S. Kozuch, S. Shaik, How to conceptualize catalytic cycles? the energetic Span model, Acc. Chem. Res. 44 (2011) 101–110.

[42] S. Kozuch, A refinement of everyday thinking: The energetic span model for kinetic assessment of catalytic cycles, Wiley Interdiscip. Rev. Comput. Mol. Sci. 2 (2012) 795–815.

[43] S.J. Hong, A.V. Virkar, Lattice parameters and densities of rare-earth oxide doped ceria electrolytes, J. Am. Ceram. Soc. 78 (1995) 433–439.

[44] D.A. Andersson, S.I. Simak, N.V. Skorodumova, I.A. Abrikosov, B. Johansson, Theoretical study of CeO_2 doped with tetravalent ions, Phys. Rev. B 76 (2007).

[45] A.K. Lucid, P.R.L. Keating, J.P. Allen, G.W. Watson, Structure and reducibility of CeO_2 doped with trivalent cations, J. Phys. Chem. C. 120 (2016) 23430–23440.

[46] S. Grieshammer, B.O.H. Grope, J. Koettgen, M. Martin, A combined DFT+*U* and Monte Carlo study on rare earth doped ceria, Phys. Chem. Chem. Phys. 16 (2014) 9974–9986.

[47] M.J.D. Rushton, A. Chroneos, Impact of uniaxial strain and doping on oxygen diffusion in CeO_2, Sci. Rep. 4 (2014) 6068.

[48] Q.L. Meng, C. Il Lee, T. Ishihara, H. Kaneko, Y. Tamaura, Reactivity of CeO_2-based ceramics for solar hydrogen production via a two-step water-splitting cycle with concentrated solar energy, Int. J. Hydrogen Energy. 36 (2011) 13435–13441.

[49] M. Ni, M.K.H. Leung, D.Y.C. Leung, Technological development of hydrogen production by solid oxide electrolyzer cell (SOEC), Int. J. Hydrogen Energy. 33 (2008) 2337–2354.

[50] C. Zhang, C.-J. Li, G. Zhang, X.-J. Ning, C.-X. Li, H. Liao, C. Coddet, Ionic conductivity and its temperature dependence of atmospheric plasma-sprayed yttria stabilized zirconia electrolyte, Mater. Sci. Eng. B. 137 (2007) 24–30.